

Study of background from accidental coincidence signals in the PandaX-II experiment

Abdusalam Abdukerim(阿布都沙拉木·阿布都克力木)¹, Wei Chen(陈葳)¹, Xun Chen(谌勋)^{*1,2}, Yunhua Chen(陈云华)³, Chen Cheng(程晨)⁴, Xiangyi Cui(崔祥仪)⁵, Yingjie Fan(樊英杰)⁶, Deqing Fang(方德清)⁷, Changbo Fu(符长波)⁷, Mengting Fu(付孟婷)⁸, Lisheng Geng(耿立升)^{9,10,11}, Karl Giboni¹, Linhui Gu(顾琳慧)¹, Xuyuan Guo(郭绪元)³, Ke Han(韩柯)¹, Changda He(何昶达)¹, Di Huang(黄迪)¹, Yan Huang(黄焱)³, Yanlin Huang(黄彦霖)¹², Zhou Huang(黄周)¹, Xiangdong Ji(季向东)¹³, Yonglin Ju(巨永林)¹⁴, Shuaijie Li(李帅杰)⁵, Huaxuan Liu(刘华萱)¹⁵, Jianglai Liu(刘江来)^{1,5,2}, Wenbo Ma(马文博)¹, Yugang Ma(马余刚)^{7,16}, Yajun Mao(冒亚军)⁸, Yue Meng(孟月)^{1,2}, Kaixiang Ni(倪恺翔)¹, Jinhua Ning(宁金华)³, Xuyang Ning(宁旭阳)¹, Xiangxiang Ren(任祥祥)¹⁵, Changsong Shang(商长松)⁵, Lin Si(司琳)¹, Guofang Shen(申国防)⁹, Andi Tan(谈安迪)¹⁵, Anqing Wang(王安庆)¹⁴, Hongwei Wang(王宏伟)^{16,17}, Meng Wang(王萌)¹⁵, Qiuhong Wang(王秋红)⁷, Siguang Wang(王思广)⁸, Wei Wang(王为)⁴, Xiuli Wang(王秀丽)¹⁴, Zhou Wang(王舟)^{1,2}, Mengmeng Wu(武蒙蒙)⁴, Shiyong Wu(吴世勇)³, Weihao Wu(邬维浩)¹, Jingkai Xia(夏经铠)¹, Mengjiao Xiao(肖梦姣)^{13,18}, Pengwei Xie(谢鹏伟)⁵, Binbin Yan(燕斌斌)¹, Jijun Yang(杨继军)¹, Yong Yang(杨勇)¹, Chunxu Yu(喻纯旭)⁶, Jumin Yuan(袁鞠敏)¹⁵, Ying Yuan(袁影)¹, Xinning Zeng(曾鑫宁)¹, Dan Zhang(张丹)¹³, Tao Zhang(张涛)^{1,2}, Li Zhao(赵力)^{1,2}, Qibin Zheng(郑其斌)¹², Jifang Zhou(周济芳)³, Ning Zhou(周宁)¹, and Xiaopeng Zhou(周小朋)⁹

¹School of Physics and Astronomy, Shanghai Jiao Tong University, MOE Key Laboratory for Particle Astrophysics and Cosmology, Shanghai Key Laboratory for Particle Physics and Cosmology, Shanghai 200240, China

²Shanghai Jiao Tong University Sichuan Research Institute, Chengdu 610213, China

³Yalong River Hydropower Development Company, Ltd., 288 Shuanglin Road, Chengdu 610051, China

⁴School of Physics, Sun Yat-Sen University, Guangzhou 510275, China

⁵Tsung-Dao Lee Institute, Shanghai 200240, China

⁶School of Physics, Nankai University, Tianjin 300071, China

⁷Key Laboratory of Nuclear Physics and Ion-beam Application (MOE), Institute of Modern Physics, Fudan University, Shanghai 200433, China

⁸School of Physics, Peking University, Beijing 100871, China

⁹School of Physics, Beihang University, Beijing 102206, China

¹⁰Beijing Key Laboratory of Advanced Nuclear Materials and Physics, Beihang University, Beijing, 102206, China

¹¹School of Physics and Microelectronics, Zhengzhou University, Zhengzhou, Henan 450001, China

¹²School of Medical Instrument and Food Engineering, University of Shanghai for Science and Technology, Shanghai 200093, China

¹³Department of Physics, University of Maryland, College Park, Maryland 20742, USA

¹⁴School of Mechanical Engineering, Shanghai Jiao Tong University, Shanghai 200240, China

¹⁵School of Physics and Key Laboratory of Particle Physics and Particle Irradiation (MOE), Shandong University, Jinan 250100, China

¹⁶Shanghai Institute of Applied Physics, Chinese Academy of Sciences, Shanghai
201800, China

¹⁷Shanghai Advanced Research Institute, Chinese Academy of Sciences, Shanghai
201210, China

¹⁸Center for High Energy Physics, Peking University, Beijing 100871, China
(PandaX-II Collaboration)

July 5, 2022

Abstract

The PandaX-II experiment employed a 580kg liquid xenon detector to search for the interactions between dark matter particles and the target xenon atoms. The accidental coincidences of isolated signals result in a dangerous background which mimic the signature of the dark matter. We performed a detailed study on the accidental coincidence background in PandaX-II, including the possible origin of the isolated signals, the background level and corresponding background suppression method. With a boosted-decision-tree algorithm, the accidental coincidence background is reduced by 70% in the dark matter signal region, thus the sensitivity of dark matter search at PandaX-II is improved.

keywords: dark matter, xenon detector, background, accidental coincidence, machine learning

1 Introduction

The direct detection of the dark matter particles, especially the weakly interacting massive particles (WIMPs), is actively carried out by a couple of experiments all over the world currently [1]. In recent years, the PandaX-II experiment located in the China Jinping Underground Laboratory (CJPL) [1, 2, 3], which uses the technology of dual phase liquid xenon time projection chambers (TPCs), has pushed the limits of cross section between WIMPs and nucleons to a new level for most of the possible WIMP masses, with other experiments of the same type [4, 5, 6, 7, 8, 9, 10]. The scattering of incident particles with xenon atoms in the TPC may produce a prompt scintillation $S1$, which resulted from the de-excitation of xenon atoms and the recombination process of some ionized electrons. Some electrons escaping from the recombination may drift along the electric field inside the TPC and be extracted into the gaseous region, producing the proportional electroluminescent scintillation $S2$ [11, 12]. The detected signals of $S1$ and $S2$ are used to reconstruct the scattering event in the data analysis. Due to the low probability of scattering events between WIMPs and ordinary matter, a good physical event requires only one pair of physically correlated $S1$ and $S2$ within the maximum electron drift time window inside the TPC. In the last results of the PandaX-I experiment [13], it was realized that the accidental coincidence of isolated $S1$ and $S2$ within the window comprises a new type of background, which contributes a number of events in the signal parameter space to search for WIMPs. Understanding this type of background and development of methods to suppress it become important for the improvement of dark matter detection sensitivity. In the data analysis of PandaX-II with the full exposure, we made a thorough study of the accidental background and presented an accurate estimation of its level for all the three data taken runs, 9, 10 and 11 [4].

In this article, we present a detailed introduction on the study of accidental background in PandaX-II. In Section 2, we provide a brief introduction to the PandaX-II TPC, the signals and the backgrounds. Then we discuss the possible origin of the accidental background in Section 3. The estimation of its level is presented in Section 4. The application of the boost-decision-tree (BDT) method to suppress the background is given in Section 5, with the performance presented. At last, we give a brief summary and outlook in Section 6.

*corresponding author, chenxun@sjtu.edu.cn

2 TPC, signals and backgrounds of PandaX-II

A detail description of PandaX-II TPC is presented in Ref. [7]. A more detailed schematic view of the TPC is presented in Figure 1. The near-cylindrical shaped TPC confined by polytetrafluoroethylene (PTFE) walls, contains both of gaseous xenon (top) and liquid xenon (bottom) in its volume. Scintillation light generated inside the TPC is detected by the two arrays of photo-multiplier tubes(PMTs) located on the top and bottom region, respectively. The cathode in the bottom part of the TPC and the gate electrode right below the liquid surface, provide the drift electric field for ionized electrons and define the sensitive region of the detector (region 1 in Figure 1).

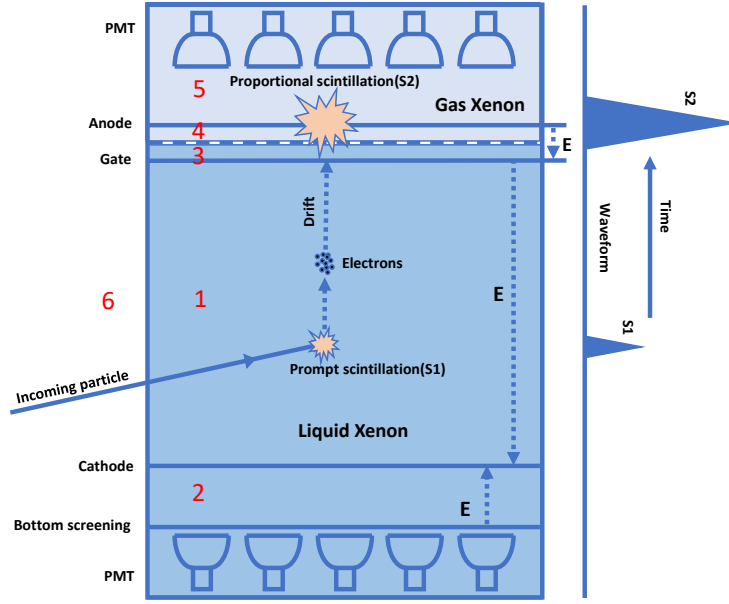


Figure 1: Schematic view of the TPC of PandaX-II, with six regions labeled with numbers: 1. the liquid part below the gate and above the cathode; 2. the liquid part below the cathode; 3. the liquid part above the gate; 4. the gas part below the anode; 5. the gas part above the anode; 6. parts outside the inner PTFE walls. A recoil event in region 1 may produce $S1$ and $S2$ signals at different regions in the detector with a time delay.

Deposited energies by scattering events inside the sensitive region result in a $S1$ signal, typically with a time spreading¹ smaller than 150 ns, in very short time, while the possible $S2$ signal will be produced after a time delay, due to the limited drift velocity of ionized electrons inside liquid xenon. The drift velocity of electrons depends only on the electric field strength, thus the time difference between physically correlated $S1$ and $S2$ can be used to calculate the vertical position of a scattering event. The maximum drift time for electrons in the sensitive region is $350 \pm 8 \mu\text{s}$ in Run 9 and $360 \pm 8 \mu\text{s}$ in Runs 10 and 11, due to the different drift fields [4]. When a “trigger” signal exceed the pre-defined threshold is observed during the ordinary data taking, the digitized waveform of all the PMTs within a window $500 \mu\text{s}$ before and after the trigger time is recorded as an event. The data processing steps calculate the baseline of each recorded waveform, search for “hit” exceeding a given threshold of 0.25 photoelectrons (PE) and cluster the overlapped hits into signals. Events of single scattering (with only one $S1$ and $S2$ reconstructed) are selected, and then filtered

¹We use the term of “width” in following text to represent this concept.

by the quality cuts to search for the possible rare scattering from WIMPs.

Recognition, understanding and suppression of the different types of backgrounds are critical in the data analysis of WIMP searching experiments because the desired signal rate is very low. In the PandaX-II experiment, the backgrounds can be categorized into four types. The electron recoil (ER) backgrounds, mainly from the radioactive isotopes in the detector material or in the xenon target, have been studied and understood with the ER calibration data and Geant4-based Monte Carlo (MC) simulations [14, 15]. The nuclear recoil (NR) background, mainly from neutrons produced by the (α, n) process or spontaneous fission of isotopes in detectors, has been estimated by the correlated high energy gamma events with the help of simulation [16]. The surface background are created by daughters of ^{222}Rn attached on the inner surface of the TPC, with suppressed $S2$ due to the charge loss on the PTFE wall. The level of surface background is estimated with a data driven method [4, 17]. The last one is the nonphysical accidental background resulted from the falsely pairing of unrelated $S1$ and $S2$ signals. A large proportion of the accidental background events have relatively small $S2$ signals, thus are not easy to be distinguished from the physical NR events (neutron or WIMPs) by investigating the ratio of $S2/S1$ only. Effective suppression of the accidental background will improve the discovery sensitivity of WIMPs greatly.

3 Origins of the accidental background

In the TPC, some $S1$ or $S2$ -like signals may be produced solely, without any other signals from the same source observed by detector. We call these signals “isolated”. Since the events with a pair of $S1$ and $S2$ are used to search for dark matter, the isolated signals appearing in the same drift window may be paired, resulting in the accidental background.

3.1 The isolated $S1$

The origins of isolated $S1$ s may be physical or non-physical. The physical origins might be in the following:

- tiny sparks on the TPC electrode, no electrons produced;
- scattering events in the region between the cathode and the screening electrode of the bottom array (region 2 in Figure 1), within which no electron could drift into the gas xenon, thus no $S2$ could be produced;
- physical events occur near the bottom wall of the detector with all electrons lost due to the imperfect of the drift field, thus no $S2$ is produced;
- scattering events above the anode in the gaseous region (region 5 in Figure 1), with no electrons entering the region below the anode to produce $S2$;
- signals produced by single electron extract into the gas region, which are mis-identified as $S1$ s;
- possible light leakage from scattering events outside the TPC (region 6 in Figure 1).

The dominant non-physical origin of isolated $S1$ is from the dark noise of the PMT, which produce small hits in the readout waveform of each PMT. During the event reconstruction, a valid signal should contain overlapped hits from at least three PMTs. The relatively high rate of dark noise (average rates are 1.9, 0.17 and 0.23 kHz per PMT for Runs 9, 10 and 11, respectively) makes it possible for the formation of small $S1$ -like signals by the randomly coincidence of the dark noises. Since these signals have contribution from the top PMTs, their top-bottom asymmetry (discussed in section 5.1) should not be -1 .

3.2 The isolated $S2$

The $S2$ signals are from the electroluminescent of electrons in the gas region. The isolated $S2$ signals, without exception, resulted from the same process. The origin of isolated $S2$ can be categorized into four types:

- real scattering event in the sensitive region with small energy deposition, and the weak $S1$ is not recognized due to the detection efficiency;

- real scattering event in the sensitive region, but it is too close to the liquid surface, resulted in overlapped $S1$ and $S2$ signals, which are recognized as one $S2$;
- real scattering event in the region above the gate but below the anode (region 3 and 4 in Figure 1), with overlapped $S1$ and $S2$ signals recognized as one $S2$; the signal may have smaller width and asymmetrical shape;
- the electrons generated with large energy deposition may not be extracted into the gas region completely. The rest electrons gather on the liquid surface and are released into the gas randomly, producing electroluminescent directly.

4 Estimation of accidental background

Since the isolated signals are independent from each other, the level of accidental background can be calculated by the rates of isolated $S1$ and $S2$ signals, assuming they follow an uniform distribution along time in a selected period with same run conditions. Estimation of the rates of these signals becomes important in this study.

For each of the data taking run, the average rates \bar{r}_1 for isolated $S1$ and \bar{r}_2 for isolated $S2$ are computed by the time weighted average of the corresponding rates:

$$\bar{r}_1 = \frac{1}{\sum_i T_i} \sum_i r_{1i} \cdot T_i, \quad (1)$$

$$\bar{r}_2 = \frac{1}{\sum_i T_i} \sum_i r_{2i} \cdot T_i, \quad (2)$$

where T_i , r_{1i} , r_{2i} are the duration, rates of isolated $S1$ and $S2$ for each selected period i , respectively. The uncertainties of the rates are calculated as the unbiased standard errors of the mean value.

4.1 Tagging of isolated $S1$

To calculate the rate of isolated $S1$, we need to recognize this type of signal correctly in the data. Three methods have been developed to search for the isolated $S1$ within the range of (3, 100) PE, which covers the energy region of searching for dark matter. One is based on a special type of “random trigger” data set, with the event triggered by hardware randomly. The other two methods are based on the dark matter search data. We describe all of these three methods here.

4.1.1 Method 1

This method is to search isolated $S1$ events in the random trigger data. The events should satisfy all the required data quality cuts mentioned in Ref. [4]. The rate r_1 in one run can be calculated easily by ²

$$r_1 = \frac{n_{iS1}}{T}, \quad (3)$$

where n_{iS1} is the number of qualified isolated $S1$, and T is the live time of the random trigger events. The method is unbiased, and is used to estimate the accidental background level in Run 10 [5]. Due to the short time of data taking with random trigger, the long term evolution of the rate can not be extracted. No random trigger data taking was performed in Run 9, so this method can only work in Runs 10 and 11.

4.1.2 Method 2

In this method, the isolated $S1$ is defined as small $S1$ signals before the triggered $S1$, which has no paired $S2$ within the window of maximum drift time (see Figure 2). The triggered $S1$ should be larger than 100 PE. The time difference Δt (see Figure 3) between the isolated $S1$ and the triggered $S1$ is used directly in the simulation of accidental background by pairing the selected isolated $S1$ and $S2$ signals (see following section), therefore we require

²The subscript “ i ” is omitted in following formulas.

that Δt should be within the window of $(10, 350) \mu\text{s}$ for Run 9 or $(10, 360) \mu\text{s}$ for Runs 10 and 11 before the triggered $S1$, respectively, by considering the cut on the drifting time.

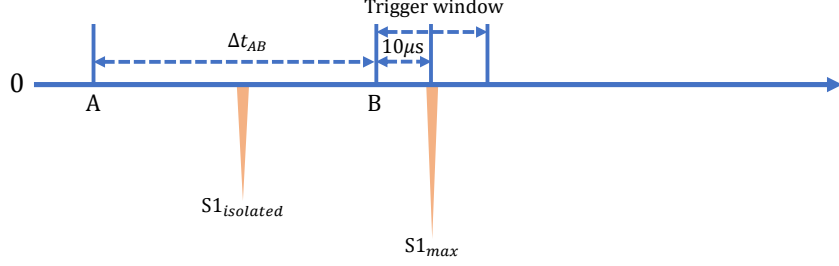


Figure 2: Schematic view on the search of isolated $S1$ in events triggered by unpaired $S1$ ($S1_{max}$) in Runs 10 and 11. The event has a fixed time window of 1 ms, and the trigger windows is within $(490, 510) \mu\text{s}$. The symbol of “A” and “B” indicates the searching window for isolated $S1$.

The rate r_1 of isolated $S1$ in one data taking period, each consisting of several adjacent runs with nearly identical running conditions, can be estimated by

$$r_1 = \frac{n_{iS1}}{n_{tS1}} \cdot \frac{1}{\Delta t_{AB}}, \quad (4)$$

where n_{iS1} is the number of isolated $S1$, n_{tS1} is the number of events triggered by unpaired $S1$, and Δt_{AB} is size of the time window, which equal to $340 \mu\text{s}$ for Run 9, and $350 \mu\text{s}$ for Runs 10 and 11, respectively. The data taking periods have similar duration.

This method was used in the first analysis of PandaX-II [6]. By studying the distribution of Δt in Figure 3, we found that the number of events decreased with the increasing Δt , indicating the possible physical correlation between some selected $S1$ s. This phenomena becomes obvious in Run 11 due to the long data taking time. The correlation may come from the ^{214}Bi - ^{214}Po cascade decay in the region below the cathode (region 2 in Figure 1). A half-life of $173.59 \pm 12.53 \mu\text{s}$ is obtained by fitting the decay component of the time distribution, and the value is consistent with the half-life of ^{214}Po ($164 \mu\text{s}$). Thus the hypothesis is supported, and method 2 results in an over-estimated rate of isolated $S1$. The average rate could be corrected by subtracting the contribution from the ^{214}Bi - ^{214}Po events, with additional uncertainty introduced by the correction.

4.1.3 Method 3

This method searches for isolated $S1$ before a good event, which is triggered by $S1$ signal larger than 100 PE and paired with $S2$ larger than 10,000 PE (see Figure 4 for details). The isolated $S1$ is required to be before the maximum drift time of the $S2$ signal, i.e., $350 \mu\text{s}$ for Run 9 and $360 \mu\text{s}$ for Runs 10 and 11, to ensure no correlation between the isolated $S1$ and the $S2$ in the good event. The cascaded decays of ^{214}Bi - ^{214}Po could not enter into the data selection because two large $S2$ signals are expected if they happen in the sensitive region.

In this method, the rate r_1 in a data taking period can be estimated as

$$r_1 = \frac{n_{iS1}}{\sum (t_{S2} - \Delta t_{A2})}, \quad (5)$$

where n_{iS1} is the total number of isolated $S1$. The variables of time are defined in each of the good event, with t_{S2} as the start time of the $S2$ signal relative to the start of the event, and Δt_{A2} as the size of the exclusion window, which takes the same value as the maximum drift time.

We studied the distribution of time difference Δt between the isolated $S1$ and the good $S1$, as shown in Figure 5. Considering the uniformity separation of the physical $S1$ and $S2$

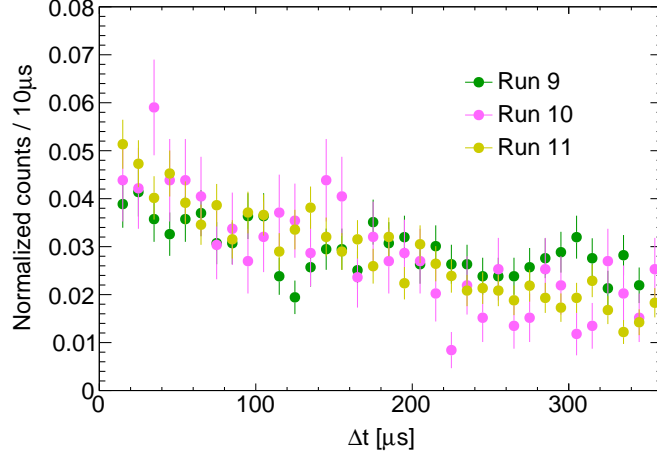


Figure 3: Distribution of the time difference Δt between the isolated $S1$ and the triggered $S1$ in method 2.

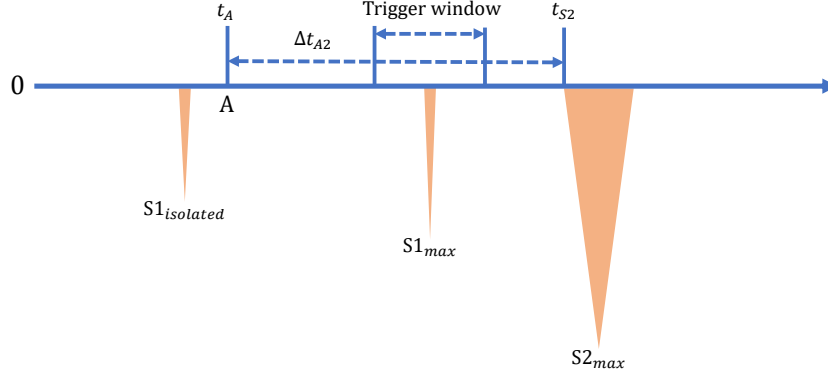


Figure 4: Schematic view on the search of isolated $S1$ in events triggered by $S1$ ($S1_{max}$) in Runs 10 and 11.

signals, the requirement of the isolated $S1$ outside the maximum drift window reduces the probability of isolated $S1$ s with small Δt to be selected. Because the selection window is reduced in the same time, the rate calculation is not affected. This behavior is reproduced with a simple toy MC simulation by randomly sampling $S2$ after the triggered $S1$ in the drift window and randomly sampling isolated $S1$ in the whole event window, especially for Run 9. The same MC simulation can also be used to verify the rate calculation. Assuming the rate of isolated $S1$ is 500 Hz, the rate calculated with method 3 is 498.9 Hz, showing a good accuracy. For Run 10, the behavior is not visible due to the relative low statistics of the isolated $S1$. For Run 11, excess isolated $S1$ s (11.6%) are observed for $\Delta t < 120 \mu s$. They are found in the events accumulated in the cathode region, as illustrated in Figure A.1 in Appendix A. The origin of these signals is still unknown.

4.2 Tagging of isolated $S2$

The estimation of the rate r_2 for isolated $S2$ is more straightforward in comparison with isolated $S1$. The events triggered by unpaired $S2$, with all the related quality cuts applied, are selected to calculate the rate. The rate is defined as

$$r_2 = \frac{n_{iS2}}{T}, \quad (6)$$

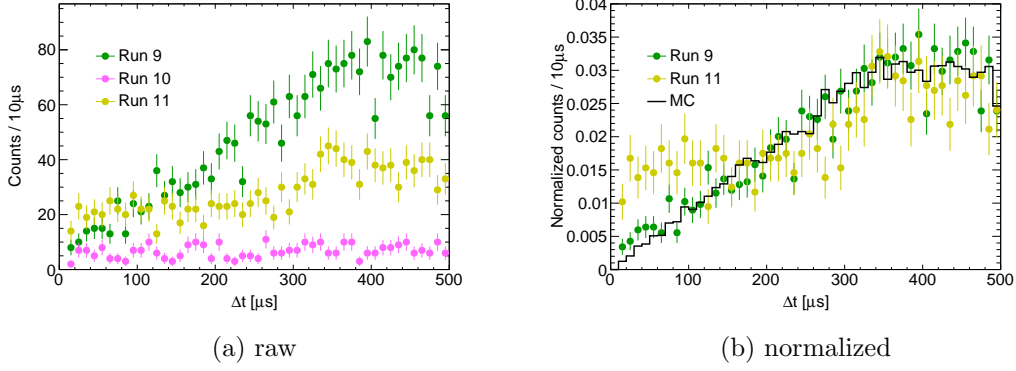


Figure 5: Distribution of the time difference Δt between the isolated $S1$ and the triggered $S1$ in method 3. **a**: Raw distribution. **b**: The integration of the distribution is normalized to 1.

where n_{iS2} is the number of events satisfying the selection criteria, and T is the duration of the run.

4.3 Properties of isolated signals

The estimated average rates of isolated $S1$ and $S2$ in each run are presented in Table 1. Run 9 has the highest rate of isolated $S1$, which is very likely to be attributed to the higher dark rate of PMTs operating with higher gain [5]. For Runs 10 and 11, the \bar{r}_1 calculated with method 1 and method 3 are consistent with each other within uncertainty. The results of method 3 are used in the final analysis of PandaX-II [4] and rest of this study to estimate the rate of accidental background. The variance of the average rates of isolated $S2$ is small.

Run	Duration [days]	\bar{r}_1 [Hz]			\bar{r}_2 [Hz]
		Method 1	Method 2	Method 3	
9	79.6	-	1.40 ± 0.25	1.53 ± 0.16	0.0121 ± 0.0002
10	77.1	0.46 ± 0.05	0.27 ± 0.20	0.47 ± 0.02	0.0130 ± 0.0007
11	244.2	0.77 ± 0.06	0.37 ± 0.16	0.69 ± 0.06	0.0121 ± 0.0001

Table 1: Average rates of isolated $S1$ and $S2$ extracted from PandaX-II data. The results from method 2 have been corrected by subtracting the contamination from the possible ^{214}Bi - ^{214}Po cascade decay signals.

More detailed evolution of rates of the isolated signals during the whole PandaX-II data taking period, with those of isolated $S1$ calculated by method 3, is presented in Figure 6. The rate of isolated $S2$ keeps stable, while that of isolated $S1$ varies greatly. The large variance of r_1 in Run 9 might come from the occasional sparking of electrodes or PMTs. A peak rate of isolated $S1$ is observed in Run 11, which can be explained by the fact that some PMTs were unstable during the corresponding period, as shown in Figure A.2 in Appendix A. The ordinary data quality cut cannot remove related events efficiently.

The charge spectra of isolated signals selected by method 3 are shown in Figure 7. Most of the isolated $S1$ are found to be smaller than 10 PE. All the $S1$ spectra have similar shape when the charge is larger than 6 PE, but a higher peak is observed below 6 PE for Run 9. This may be explained by the higher chance of accidental coincidence of hits from dark current in this run due to the higher operation voltage of the PMTs. A small peak in Run 11 around 10 PE is resulted from the unstable PMTs mentioned before (see Figure A.3 in Appendix A). The spectra of isolated $S2$ are consistent with each other.

4.4 Study of the accidental background with simulation

A data-driven MC simulation with the selected isolated signals is used to study the accidental background events. For each Run, the isolated $S1$ and $S2$ are paired randomly,

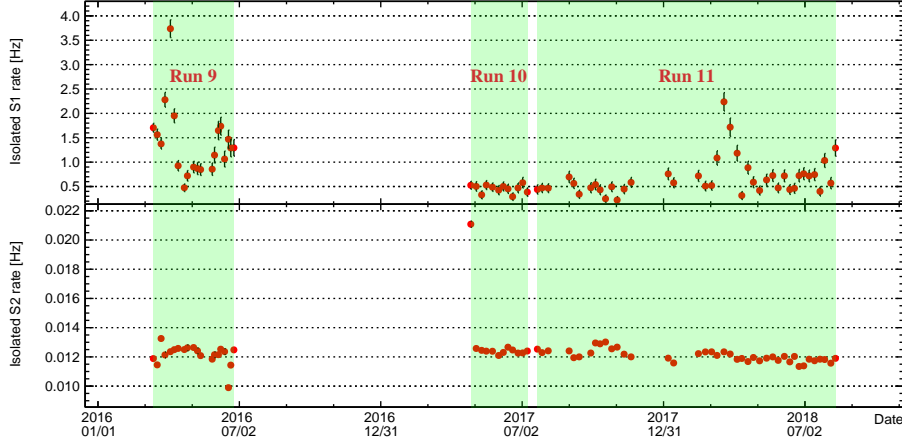


Figure 6: Evolution of rates of the isolated signals during the whole PandaX-II data taking period, selected by method 3.

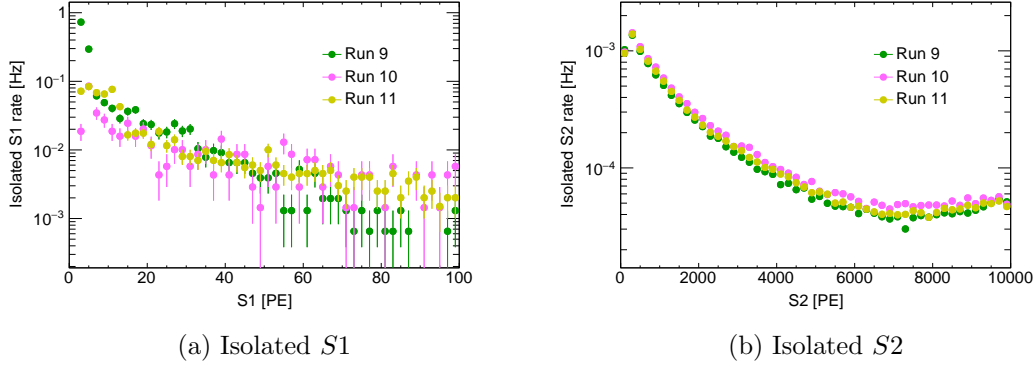


Figure 7: Charge spectra of isolated signals selected by method 3.

with the time separation between them sampled uniformly in the time window Δt_w defined by the fiducial volume cut. The horizontal position of the event is determined by the $S2$ signal. The paired mock event is treated as an event with raw signals. The same position-dependent charge corrections and quality cuts for dark matter search data are applied to these events, resulted in a cut efficiency ϵ .

Then the total number n_{acc} of accidental background events can be calculated by

$$n_{acc} = \bar{r}_1 \cdot \bar{r}_2 \cdot \Delta t_w \cdot T \cdot \epsilon. \quad (7)$$

The efficiency ϵ , the total number of accidental events, and the number of events below the median line of the NR band from calibration data [4] results, are presented in Table 2. Run 11 has the larger number of accidental background events due to the largest duration T .

The distributions of $\log_{10}(S2/S1)$ vs. $S1$ for the simulated accidental background events after all the quality cuts within the dark matter search window [4] are given in Figure 8, together with those of the NR calibration data. Most of the accidental events have a relative small $S1$ charge and are above the NR median. Considering the low statistics of the most critical ER backgrounds below the NR median, the non-negligible accidental background in this region will reduce the discovery power for WIMPs. Suppressing these background could improve the sensitivity of the detector for WIMP search.

Run	Type	ϵ	n_{acc}
9	total	21.9%	8.15 ± 0.94
	below NR median	3.5%	1.31 ± 0.15
10	total	25.6%	3.16 ± 0.15
	below NR median	8.5%	1.06 ± 0.05
11	total	18.2%	9.87 ± 0.89
	below NR median	5.6%	2.93 ± 0.27

Table 2: Number of accidental events estimated with the selected isolated signals using method 3.

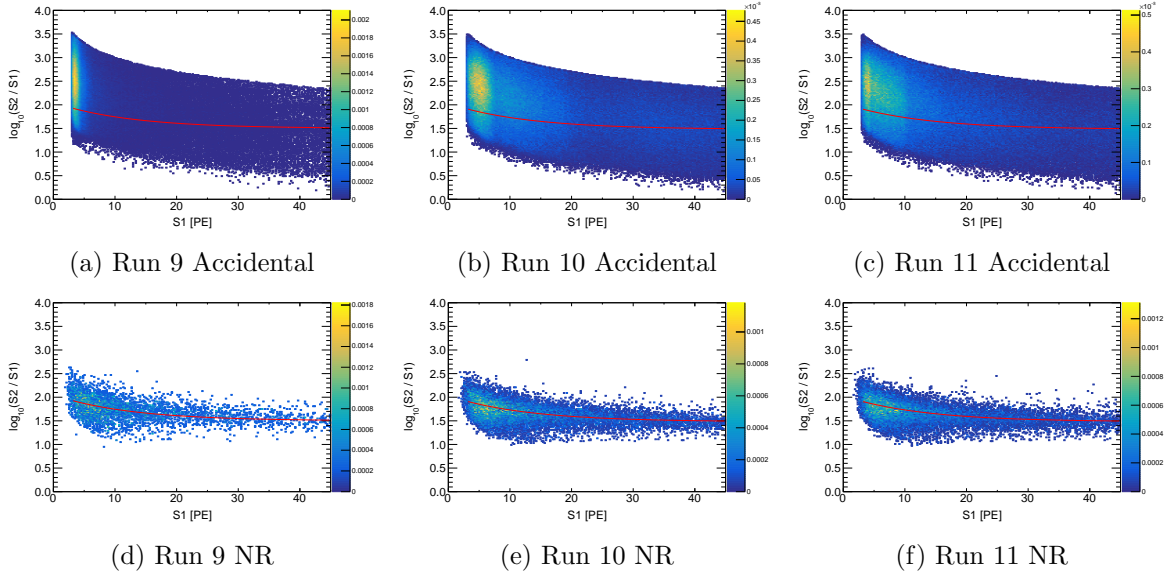


Figure 8: Distribution of $\log_{10}(S2/S1)$ vs. $S1$ for the simulated accidental background and NR calibration data. The red curves are the corresponding NR median for each Run.

5 Suppression of accidental background with BDT

The accidental events are composed with isolated $S1$ and $S2$. Since there are no physical correlation between them, we would expect a method to distinguish them from the physical events by considering the joint distributions of the properties of these signals. Because all the selected accidental events have passed the quality cuts, it is hard to tell the difference between any single property of a signal from the accidental events and the physical events. A multi-variant analysis could be used. The algorithm of BDT, as one of the most successful multi-variant analysis method used in particle physics [18], was firstly used to suppress the accidental background in the first analysis results of PandaX-II [6]. The real signal of the WIMP-nucleon scattering is NR, thus the single scattering events from NR calibration runs (AmBe) should be used as input signals in the machine learning, with randomly paired events as backgrounds. Given the fact that the ER events dominate the region above the NR median in the dark matter search data and the relative low estimated number of accidental events in the region, we only consider to distinguish the accidental background from the physical NR events below the NR median.

5.1 Variables

The TMVA (Toolkit for Multivariate Data Analysis) package in ROOT is used to perform the BDT machine learning [19]. A set of signal properties are exploited to search for the difference between the accidental events and the physical NR events, including

- corrected charge of $S1$ (qS1);
- corrected charge of $S2$ (qS2);
- raw charge of $S1$ (qS1R);
- raw charge of $S2$ (qS2R);
- width of $S2$ (wS2);
- full width at tenth maximum of $S2$ (wTenS2);
- asymmetry between the top charge and the bottom charge for $S1$ (S1TBA);
- ratio of the top charge to the bottom charge for $S2$ (S2TBR);
- the ratio of the pre-max-height charge to the total charge of an $S2$ signal (S2SY1 in the directly summed over waveform, S2SY2 in the smoothed waveform);
- number of local maximums (peaks) of $S1$ (S1NPeaks);
- ratio of the largest charge collected by the bottom PMT of $S1$ to total charge of $S1$ (S1LargestBCQ)

Distributions of the these variables for the events below the NR median can be found in Figure 9, and their correlations are presented in Figure A.5.

5.2 BDT results

We constructed the adaptive BDT using the default parameters provided by the official ROOT TMVA classification example, except the parameter of **NTrees** (number of trees). We trained the data for the three runs independently, each with a predefined set of **NTrees**. After the training, the resulted BDT response distributions of the training and test data samples are superimposed and the Kolmogorov-Smirnov (K-S) test is performed to check for overtraining (see Fig. A.4 for details). We choose **NTrees** = 90 for further study. With the trained BDT, the “likelihood” estimators can be calculated for an input event to be classified. The best cut criteria for the estimator is obtained with the test data set by maximizing the significance S ,

$$S = \frac{\epsilon_s n_s}{\sqrt{\epsilon_s n_s + \epsilon_b n_b}}, \quad (8)$$

where n_s and n_b are the number of signal and background events, respectively, ϵ_s and ϵ_b are the efficiencies for signal and background events at a given estimator value, respectively. In this study, the expected signal events below the NR median have high probability to be the neutron background or the WIMP events, they are estimated at the same level as the accidental background [4]. Therefore, the identical numbers of n_s and n_b are used to calculate the significance. The evolution of the background rejection efficiency with the signal efficiency at different BDT cut values is shown in Figure 10. The results at the maximum significance S are presented in Table 3. The BDT algorithm is capable to remove 70% of the accidental background events, while keeping about 90% of the single scattering NR events below the NR median curve in all of the three runs. The distributions of the BDT cut efficiency on the $\log_{10}(S2/S1)$ vs. $S1$ plane for the simulated accidental background are given in Figure 11.

Run	S	ϵ_s	$1 - \epsilon_b$
9	25.9	90.4%	70.2%
10	26.5	91.1%	74.6%
11	26.2	90.7%	73.7%

Table 3: The significance S , signal efficiencies ϵ_s and background rejection efficiencies $1 - \epsilon_b$ at the best cut value of the estimator for events below the NR median lines, assuming $n_s = n_b$.

The contribution of each input variable to the discrimination power is extracted by the BDT training. The variables of wS2, S2SY2, S1TBA are found to be the most critical to the recognition of accidental backgrounds. By checking the distributions of these variables,

isolated $S2$ signals are found to have smaller width ($wS2$) and more asymmetrical shape ($S2SY2$) in comparison with those in normal events, indicating that most of these signals are generated near the grid wires [20]. The peak in the $S1TBA$ distribution of physical events at the value of -1 suggests a large fraction of the physical $S1$ signals have no hits on the top PMT array. Given the fact that physical $S1$ s are produced inside the liquid xenon, small signals have smaller chance to be detected by the top PMTs due to the total reflection on the surface between the liquid and gas xenon. But some of the non-physical $S1$ s are from the coincidence of dark noises on the top PMTs, resulted in a $S1TBA$ larger than -1. The distribution of $S1TBA$ could be used to estimate the fraction of isolated $S1$ s from the coincidence of dark noise from top PMTs. This phenomenon helps to distinguish the non-physical small $S1$ signals from the real ones.

5.3 Overall results

In the analysis, the BDT cut is not only applied to the events below the NR median, but applied to all the events in the search window. The efficiencies of BDT to different types of events are extracted by using the calibration data sets, shown in Figure 12. The BDT cut efficiencies for the ER and NR calibration data expressed as functions of $S1$, are used to build the final signal model [21]. The efficiencies for ER events are lower than those of NR events when $S1 < 8$ PE, in all of the data set. From the 2D efficiency maps, it is observed that in the region of low $S1$, the ER events with a higher ratio of $S2/S1$ are suppressed heavily in Runs 10 and 11. On the contrary, more ER events with smaller $S2/S1$ in the same region are suppressed in Run 9. The different distributions of $S2$ related variables of the different ER calibration data may result in the different efficiencies. The distribution of $\log_{10}(S2/S1)$ vs. $S1$ of accidental background after the BDT cut are used directly in the model.

The expected numbers of accidental background (below NR median) in PandaX-II full exposure data set after the BDT cuts are 2.09 ± 0.25 (0.39 ± 0.05), 1.03 ± 0.05 (0.27 ± 0.01) and 2.53 ± 0.24 (0.77 ± 0.07) for Runs 9, 10, and 11, respectively. The total number of expected accidental background events below NR median is smaller than 1.5. Considering that the total data taking period of PandaX-II is 244.2 days, we have successfully suppressed the accidental background to a trivial level and improved the final sensitivity for dark matter search [4].

6 Summary and Outlook

The accidental background is an important composition of the backgrounds in the dark matter search experiments with dual phase xenon detector. We discussed the possible origins of the two components, isolated $S1$ and $S2$, and developed methods to estimate the level of accidental background in the PandaX-II experiment. The BDT algorithm is used to distinguish this non-physical background from real NR signals below the NR median lines, so that the level of this background is suppressed greatly.

We found that the rate of isolated $S1$ is much higher in Run 9, during which the PMTs are running with higher gains than in other runs. This suggests the coincident combination of hits created by dark noise contributes a large amount to the isolated $S1$. Thus reducing the dark noise of PMTs is critical for next generation of experiments [22, 23, 24].

The BDT method works well in the suppression of the accidental background in our study. The analysis framework and suppression method can be used in the data analysis of the subsequent PandaX-4T experiment [25]. Because the number of accidental events is nearly proportional to the operation time, only a few of them have been produced in the commissioning run. They have been suppressed to a very low level with the quality cuts and therefore this method is not used in the first PandaX-4T WIMP search. But PandaX-4T and other similar experiments will be running much longer than PandaX-II, our study provides a valuable reference to them. With the rapid development of the machine learning methods in recent year, we may expect the methods of neural networks or some others may achieve equivalent success in this topic.

Acknowledgment

This project is supported in part by a grant from the Ministry of Science and Technology of China (No. 2016YFA0400301), grants from National Science Foundation of China (Nos. 12090060, 12005131, 11905128, 11925502, 11775141), and by Office of Science and Technology, Shanghai Municipal Government (grant No. 18JC1410200). We thank supports from Double First Class Plan of the Shanghai Jiao Tong University. We also thank the sponsorship from the Chinese Academy of Sciences Center for Excellence in Particle Physics (CCEPP), Hongwen Foundation in Hong Kong, and Tencent Foundation in China. Finally, we thank the CJPL administration and the Yalong River Hydropower Development Company Ltd. for indispensable logistical support and other help.

References

- [1] J. Liu, X. Chen and X. Ji, *Current status of direct dark matter detection experiments*, *Nature Phys.* **13** (2017) 212.
- [2] K. J. Kang et al., *Status and prospects of a deep underground laboratory in China*, *J. Phys. Conf. Ser.* **203** (2010) 012028.
- [3] L. Zhao and J. Liu, *Experimental search for dark matter in China*, *Front. Phys. (Beijing)* **15** (2020) 44301 [2004.04547].
- [4] PANDAX-II collaboration, *Results of dark matter search using the full PandaX-II exposure*, *Chin. Phys. C* **44** (2020) 125001 [2007.15469].
- [5] PANDAX-II collaboration, *Dark Matter Results From 54-Ton-Day Exposure of PandaX-II Experiment*, *Phys. Rev. Lett.* **119** (2017) 181302 [1708.06917].
- [6] PANDAX-II collaboration, *Dark Matter Results from First 98.7 Days of Data from the PandaX-II Experiment*, *Phys. Rev. Lett.* **117** (2016) 121303 [1607.07400].
- [7] PANDAX collaboration, *Dark Matter Search Results from the Commissioning Run of PandaX-II*, *Phys. Rev.* **D93** (2016) 122009 [1602.06563].
- [8] LUX collaboration, *Results from a search for dark matter in the complete LUX exposure*, *Phys. Rev. Lett.* **118** (2017) 021303.
- [9] XENON collaboration, *Dark Matter Search Results from a One Ton-Year Exposure of XENON1T*, *Phys. Rev. Lett.* **121** (2018) 111302.
- [10] XENON collaboration, *First Dark Matter Search Results from the XENON1T Experiment*, *Phys. Rev. Lett.* **119** (2017) 181301 [1705.06655].
- [11] E. Aprile and T. Doke, *Liquid Xenon Detectors for Particle Physics and Astrophysics*, *Rev. Mod. Phys.* **82** (2010) 2053 [0910.4956].
- [12] E. Aprile, C. E. Dahl, L. DeViveiros, R. Gaitskell, K. L. Giboni, J. Kwong et al., *Simultaneous measurement of ionization and scintillation from nuclear recoils in liquid xenon as target for a dark matter experiment*, *Phys. Rev. Lett.* **97** (2006) 081302 [astro-ph/0601552].
- [13] PANDAX collaboration, *Low-mass dark matter search results from full exposure of the PandaX-I experiment*, *Phys. Rev. D* **92** (2015) 052004 [1505.00771].
- [14] GEANT4 collaboration, *GEANT4—a simulation toolkit*, *Nucl. Instrum. Meth. A* **506** (2003) 250.
- [15] J. Allison et al., *Geant4 developments and applications*, *IEEE Trans. Nucl. Sci.* **53** (2006) 270.
- [16] PANDAX-II collaboration, *An Improved Evaluation of the Neutron Background in the PandaX-II Experiment*, *Sci. China Phys. Mech. Astron.* **63** (2020) 231011 [1907.00545].
- [17] D. Zhang, *Estimating the surface backgrounds in PandaX-II WIMP search data*, *JINST* **14** (2019) C10039.

- [18] B. P. Roe, H.-J. Yang, J. Zhu, Y. Liu, I. Stancu and G. McGregor, *Boosted decision trees, an alternative to artificial neural networks*, *Nucl. Instrum. Meth. A* **543** (2005) 577 [[physics/0408124](#)].
- [19] A. Hocker et al., *TMVA - Toolkit for Multivariate Data Analysis*, [physics/0703039](#).
- [20] LUX collaboration, *Improving sensitivity to low-mass dark matter in LUX using a novel electrode background mitigation technique*, *Phys. Rev. D* **104** (2021) 012011 [[2011.09602](#)].
- [21] PANDAX-II collaboration, *Determination of responses of liquid xenon to low energy electron and nuclear recoils using a PandaX-II detector*, *Chin. Phys. C* **45** (2021) 075001 [[2102.09158](#)].
- [22] PANDAX collaboration, *Dark matter direct search sensitivity of the PandaX-4T experiment*, *Sci. China Phys. Mech. Astron.* **62** (2019) 31011.
- [23] B. J. Mount et al., *LUX-ZEPLIN (LZ) Technical Design Report*, [1703.09144](#).
- [24] XENON collaboration, *Projected WIMP sensitivity of the XENONnT dark matter experiment*, *JCAP* **11** (2020) 031.
- [25] PANDAX-4T collaboration, *Dark Matter Search Results from the PandaX-4T Commissioning Run*, *Phys. Rev. Lett.* **127** (2021) 261802 [[2107.13438](#)].

A Complementary plots

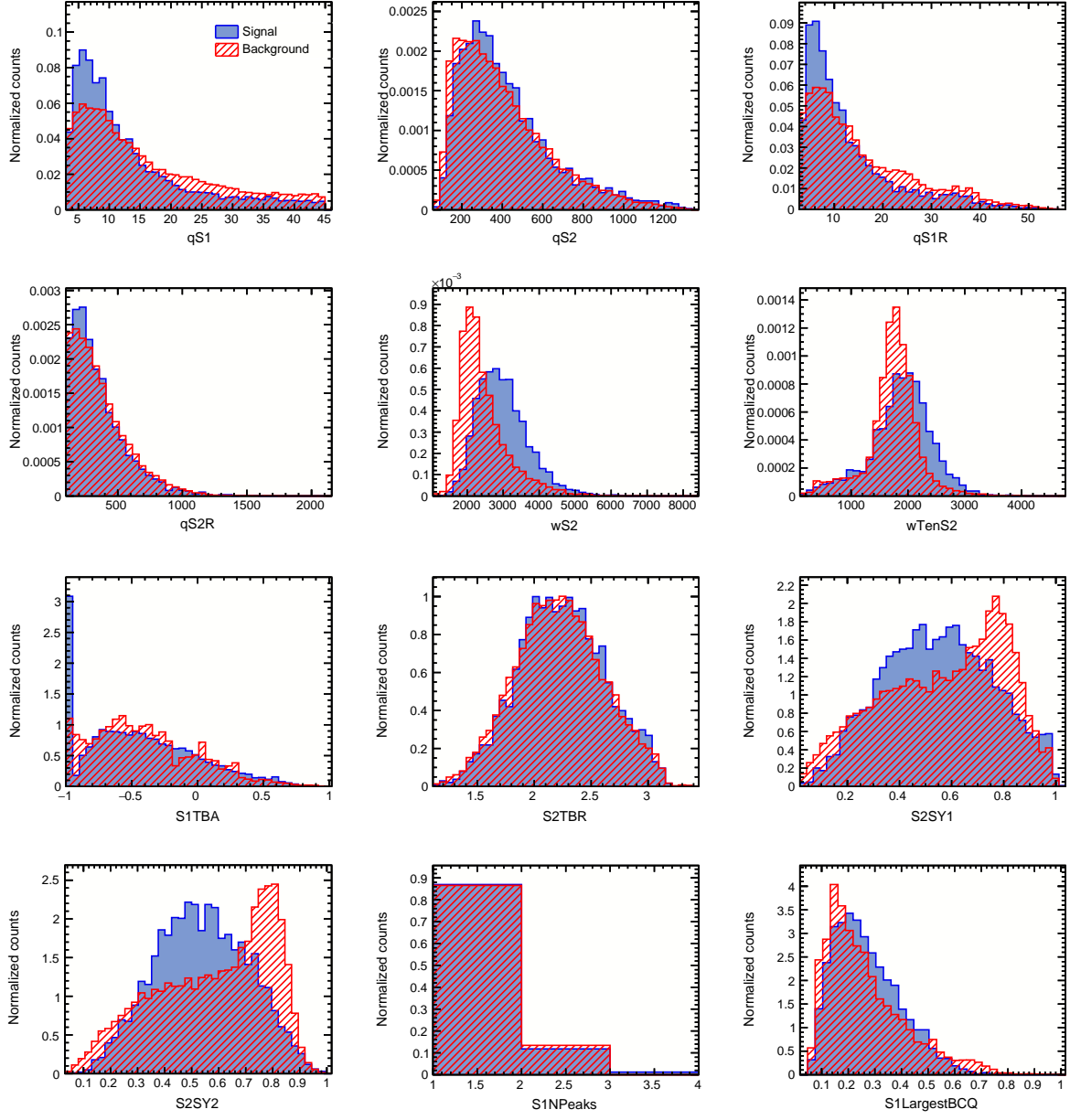


Figure 9: Distribution of the selected variables from the NR calibration data (signal) and the simulated accidental events (background) in Run 11. Only the events below the NR median are selected.

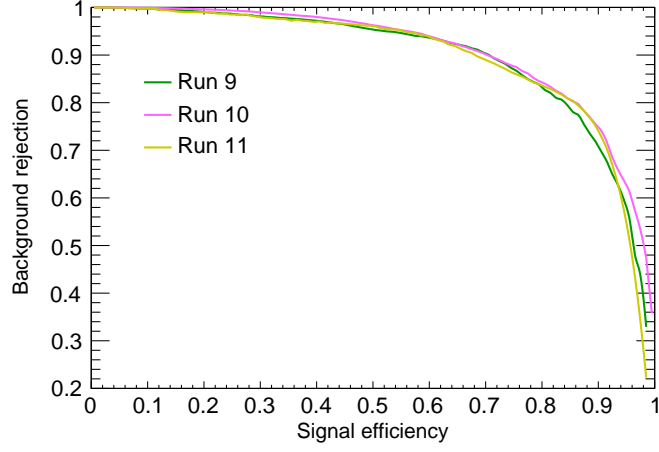


Figure 10: The evolution of the background rejection efficiency with the signal efficiency at different BDT cuts for different runs. The initial numbers of background and signal events are assumed to be identical.

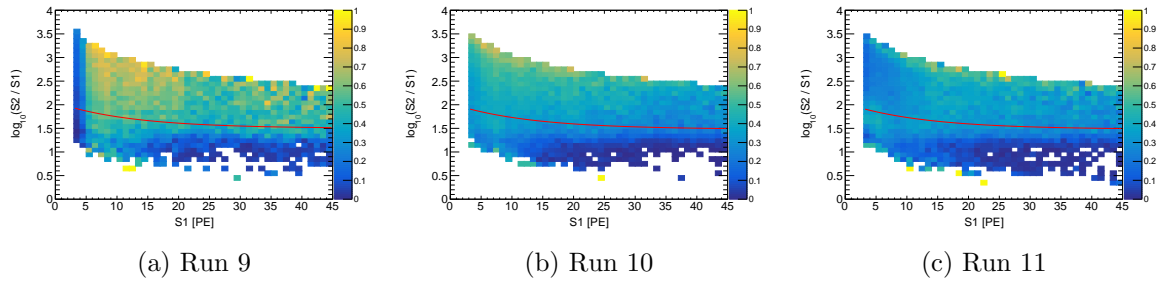


Figure 11: BDT cut efficiency map on the $\log_{10}(S2/S1)$ vs. $S1$ distribution for the simulated accidental background.

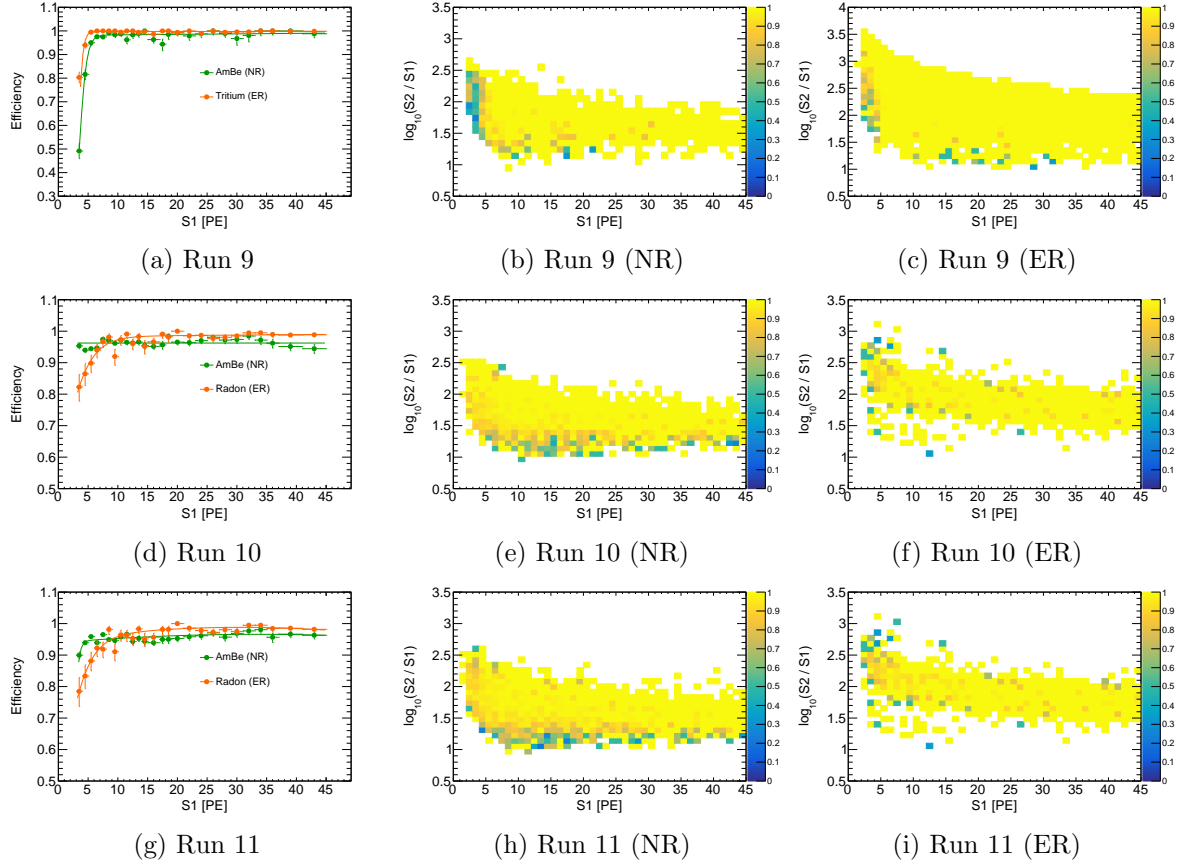


Figure 12: The BDT cut efficiency curves as a function of $S1$ and efficiency maps on the $\log_{10}(S2/S1)$ versus $S1$ for different calibration data in the dark matter search window for different Runs.

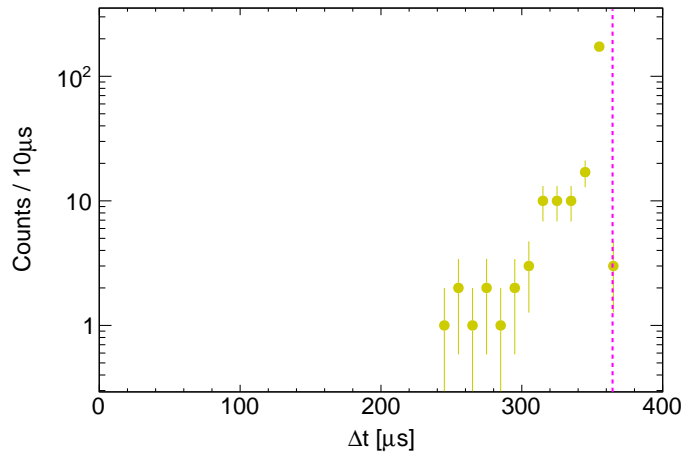


Figure A.1: Distribution of the time difference between $S1_{max}$ and $S2_{max}$ at the condition where time difference between the isolated $S1$ and $S1_{max}$ is smaller than $120 \mu s$ ($\Delta t < 120 \mu s$) in method 3. The pink dashed line represents the maximum drift time.

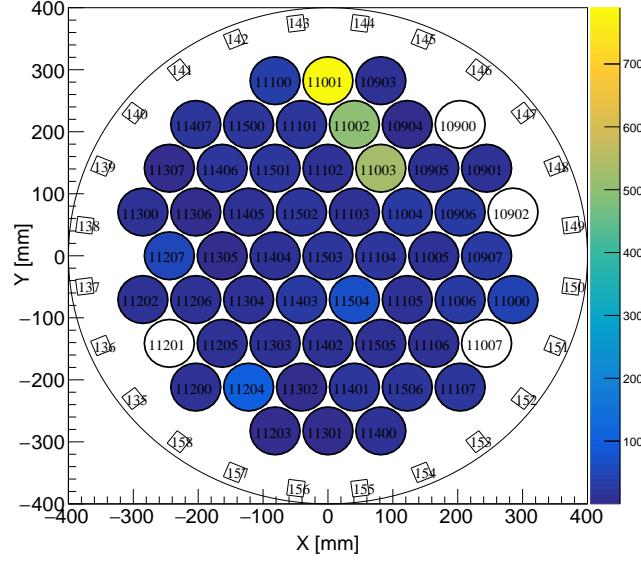


Figure A.2: Accumulated charge pattern in the top PMT array of all isolated S1s from Mar. 11, 2018 to Apr. 6, 2018. Three PMTs are observed to have the largest contribution to these signals.

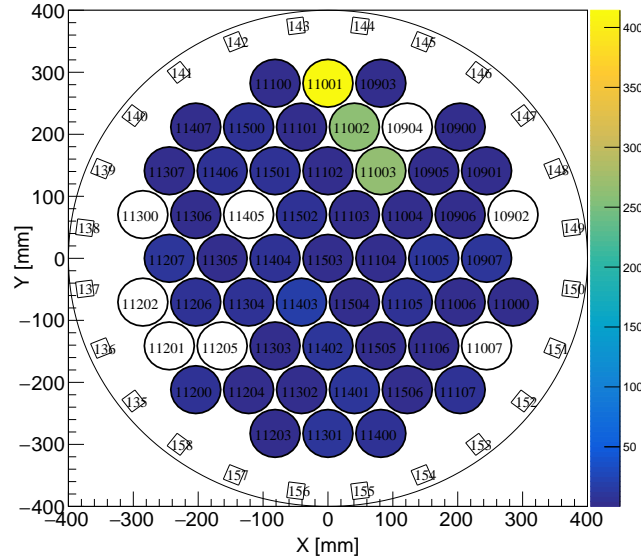


Figure A.3: Accumulated charge pattern in the top PMT array of isolated S1s in the window of (10,12) PE in Run 11. Three PMTs are observed to have the largest contribution to these signals.

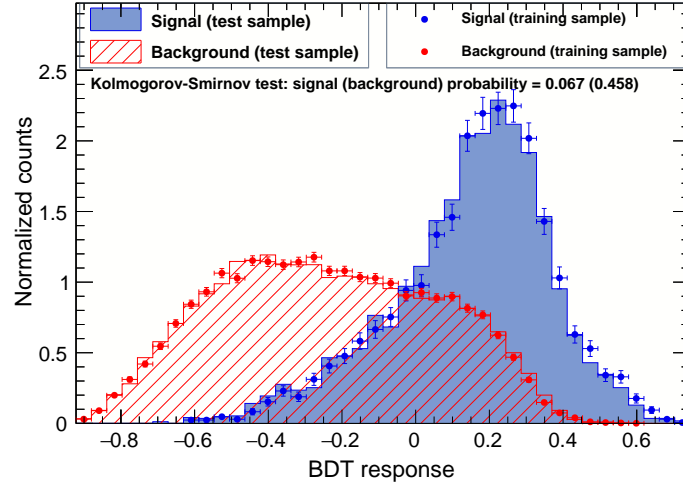
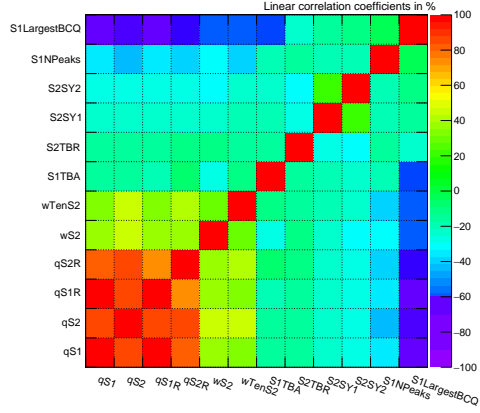
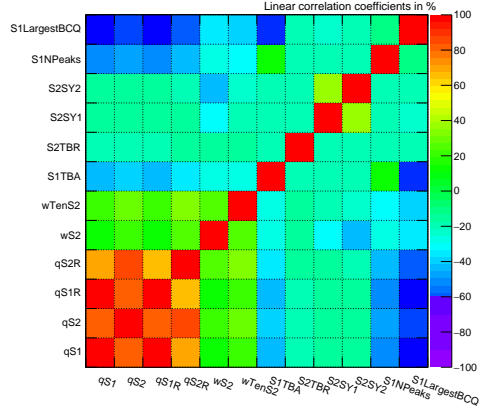


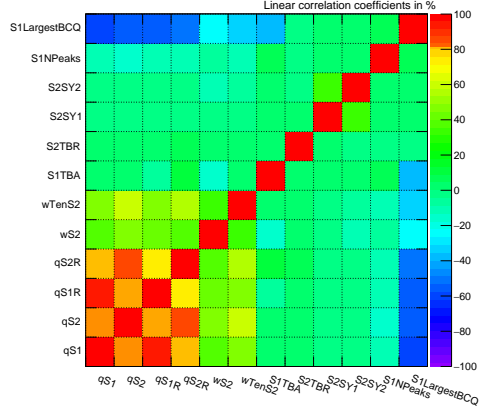
Figure A.4: The distributions of BDT response of the train and test data samples. The K-S test probabilities are used to indicate the overtraining.



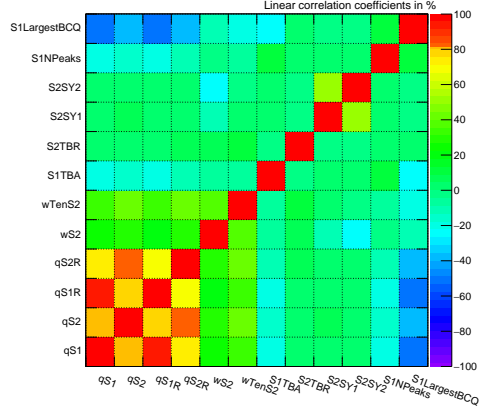
(a) Run 9 (Signal)



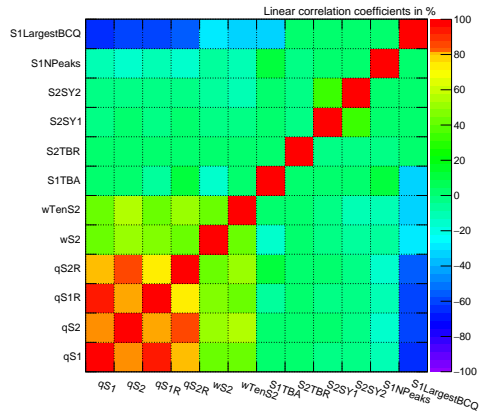
(b) Run 9 (Background)



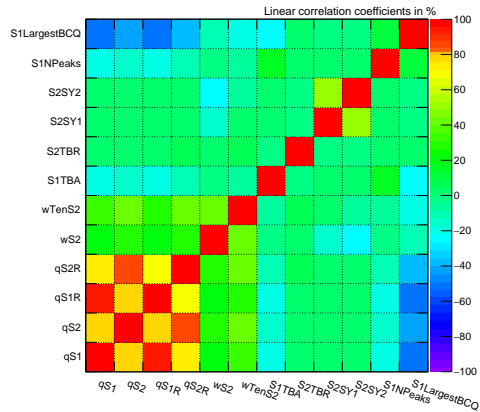
(c) Run 10 (Signal)



(d) Run 10 (Background)



(e) Run 11 (Signal)



(f) Run 11 (Background)

Figure A.5: Correlations between the variables used for BDT training, from the events below the NR median.